The deglaciation of Barton Peninsula (King George Island, South Shetland, Antarctica) based on geomorphic evidence and lacustrine records

Journal:	*Polar Record*
Manuscript ID	POL-RA-2019-0026.R1
Manuscript Type:	Research Article
Keywords:	Barton Peninsula, geomorphology, lake records, deglaciation, tephrostratigraphy

Marc Oliva[1] , Dermot Antoniades[2], Enrique Serrano[3], Santiago Giralt[4], Emma J. Liu[5], Ignacio Granados[6], Sergi Pla-Rabes[7], Manuel Toro[8], Soon Gyu Hong[9], and Gonçalo Vieira[10]

[1]Department of Geography, University of Barcelona, Spain; [2]Department of Géographie & Centre d'Études Nordiques, Université Laval, Canada; [3]Department of Geography, University of Valladolid, Spain; [4]Institute of Earth Sciences Jaume Almera, CSIC, Spain; [5]Department of Earth Sciences, University of Cambridge, UK; [6]Centro de Investigación, Seguimiento y Evaluación, Spain; [7]Centre de Recerca Ecològica i Aplicacions Forestals (CREAF), Spain; [8]Centre for Hydrographic Studies (CEDEX), Spain; [9]Korea Polar Research Institute, South Korea and [10]Centre for Geographical Studies – IGOT, Universidade de Lisboa, Portugal

Abstract

Barton Peninsula is an ice-free area located in the southwest corner of King George Island (South Shetland Islands, Antarctica). Following the Last Glacial Maximum, several geomorphological features developed in newly exposed ice-free terrain and their distribution provide insights about past environmental evolution of the area. Three moraine systems are indicative of three main glacial phases within the long-term glacial retreat, which also favoured the development of numerous lakes. Five of these lakes were cored to understand in greater detail the pattern of deglaciation through the study of lacustrine records. Radiocarbon dates from basal lacustrine sediments enabled the reconstruction of the chronology of Holocene glacial retreat. Tephra layers present in lake sediments provided additional independent age constraints on environmental changes based on geochemical and geochronological correlation with Deception Island-derived tephra. Shrinking of the Collins Glacier exposed the southern coastal fringe of Barton Peninsula at 8 cal ky BP. After a period of relative stability during the mid-Holocene, the ice cap started retreating northwards after 3.7 cal ky BP, confining some glaciers within valleys as shown by moraine systems. Lake sediments confirm a period of relative glacial stability during the last 2.4 cal ky BP.

1. INTRODUCTION

Climate records from ice cores and geomorphological and sedimentological evidence show that the temperature increase following the Last Glacial Maximum (LGM) began on the Antarctic continent at 18 ky (Denton et al. 2010; Stenni et al. 2011; Bentley et al. 2014). One of the main environmental consequences of this warming was the appearance of ice-free areas in regions of the Maritime Antarctic where the Equilibrium Line Altitude (ELA) was close to sea level. This glacial retreat was clearly observed in the South Shetland Islands (SSI), where present-day mean annual air temperatures at sea level are between -1 and -2 ºC (Oliva et al. 2017a).

Based on currently available geochronological data (mostly from lacustrine and marine records), the deglaciation of the northern fringe of the western Antarctic Peninsula region started between 14 and 15 cal ky BP and continued throughout the Holocene (Ingólfsson, Hjort, & Humlum, 2003; Ó Cofaigh et al. 2014). In the case of the SSI, the margins of the largest deglaciated areas became ice-free during the Early Holocene, as inferred from lake records in Fildes Peninsula, King George Island (Watcham et al. 2011) and Byers Peninsula, Livingston Island (Toro et al. 2013; Oliva et al. 2016). Surface exposure dating using atmospheric ^{36}Cl on Barton Peninsula, King George Island, suggested that the remaining ice caps (which still cover 85-90% of the SSI) started thinning at 15.5 ky, which continued throughout the Holocene (Seong et al. 2009). This timing is in agreement with marine records from Maxwell Bay, King George Island, which indicate that glacial retreat began between 14.1 and 14.8 cal ky BP (Milliken, Anderson, Wellner, Bohaty, & Manley, 2009; Simms, Milliken, Anderson, & Wellner, 2011), or potentially earlier at 17 cal ky BP (Yoon, Han, Park, Oh, & Chang, 1997). The implications of this retreat for both terrestrial and marine ecosystems were significant, and included changes in the distribution of vegetation (Fretwell, Hodgson, Watcham, Bentley, & Roberts, 2010) and changing geomorphological dynamics (López-Martínez, Serrano, Schmid, Mink, & Linés, 2012; Oliva & Ruiz-Fernández, 2015; Ruiz-Fernández & Oliva, 2016; Ruiz-Fernández et al. 2019).

This study focuses on Barton Peninsula, an ice-free area in the SW corner of King George Island, northern SSI. Our aim is to expand our understanding of the deglaciation process in this peninsula through the integrated study of both geomorphic features and lake sediment records. Geomorphological observations reveal a sequence of environmental stages that took place following the onset of deglaciation. Furthermore, we describe lacustrine

sedimentary sequences and tephrostratigraphy from five lakes distributed around the peninsula; we present radiocarbon dates indicative of the onset of lacustrine sedimentation and therefore of glacial retreat; and we improve the chronological framework of the deglaciation process in the Barton Peninsula by providing new ages for its south-eastern region, where cosmogenic dates are lacking.

2. STUDY AREA

King George Island is the largest island in the SSI archipelago. Glaciers cover more than 90% of its total area (Osmanoğlu, Braun, Hock, & Navarro, 2013). Aside from the Fildes Peninsula – the island's largest ice-free area – there are several small ice-free enclaves along the margins of this island, of which Barton Peninsula is one. This peninsula, located between Maxwell Bay and Collins Glacier has a rough orography with elevations exceeding 290 m asl (Fig. 1).

The retreat of Collins Glacier during the Holocene exposed an ice-free area of ca. 8 km^2, where numerous lakes are distributed in glacial depressions and/or dammed by moraines (Fig. 1). Several of these lakes were cored for paleoenvironmental purposes (Fig. 2, Table 1).

Figure 1

Instrumental climate records at the South Korean King Sejong Station at 11 m asl between 1998 and 2014 showed a mean annual temperature of -1.8 ºC and an annual precipitation of 598 mm (1988-2014). Barton Peninsula is predominantly composed of igneous rocks (extrusive volcanics and intrusive granites) of Paleogene age that are heavily weathered where exposed (Davies, 1982, Lee et al. 2002). The peninsula has been intensely shaped by glaciers, periglacial, marine, and tectonic processes, with the formation of several raised marine platforms between sea level and the highest peaks (López-Martínez, Serrano, & Lee, 2002; Serrano & López-Martínez, 2004). In the ice-free areas of the SSI, periglacial processes are widespread. Permafrost is sporadic near the coast, with rock glaciers showing the lowest permafrost patches, and becoming continuous only at higher elevations (Vieira et al. 2010; Bockheim et al. 2013; Correia, Oliva, Ruiz-Fernández, 2017; Oliva et al.

2017b; Hrbáček et al., 2018). The vegetation cover of the peninsula is scarce and comprises small patches of grass, and prevailing communities of mosses and lichens (Ruiz-Fernández, Oliva, García-Hernández, 2017).

Figure 2

Table 1

3. MATERIALS AND METHODS

3.1 Geomorphology

Geomorphological mapping was conducted in the summer when the landscape was free of snow and landforms features were clearly visible. We mapped the landforms and deposits in the field at 1:10000 scale, and presented the resulting map in López-Martínez et al. (2002). Here, we use the main geomorphological units identified in that map as the basis from which to reconstruct past glacial phases in Barton Peninsula. The geomorphological sketch presented in Fig. 3 includes the main moraine systems, marine platforms and raised beaches as well as the distribution of lakes.

3.2 Lake sediments

Five lakes from Barton Peninsula were cored from January to February 2012 (see Table 1), using a gravity/percussion corer deployed from an inflatable boat. The sediment cores were stored at + 4 ºC in a dark room until opened at the Institute of Earth Sciences Jaume Almera (ICTJA-CSIC, Barcelona, Spain). A moss sample was radiocarbon dated in lake L12, but due to a lack of moss remnants, bulk sediment samples from the bottom of the other cores were processed for ^{14}C Accelerator Mass Spectrometry (AMS)-dating at the Beta Analytic (Miami, USA) and Centro Nacional de Aceleradores (Seville, Spain) laboratories. Radiocarbon dates were calibrated using CALIB 7.1 with the SHCal13 calibration curve (Reimer et al. 2013) and selecting the median of the 95.4 % distribution (± 2σ probability interval; see Table 2).

Table 2

3.3 Tephrochronology

Tephra, in the form of ash-sized volcanic material, was sampled from six visible layer from lacustrine records: three from lake L6 and three from lake L5. Samples were cleaned in an ultrasonic bath for five minutes to remove organic material and dried overnight in an oven at 80 ˚C. Dried samples were sieved to separate material >125 μm, which was uncontaminated by disaggregated organic material, and mounted in epoxy resin. Major element compositions in matrix glass were measured on carbon-coated polished grain mounts using the Cameca SX100 electron microprobe (EPMA) at the University of Bristol, UK. Analyses were performed under operating conditions of 15 kV accelerating voltage and 4 nA beam current using a defocused beam (10 μm) to minimise sodium mobility. A combination of mineral and glass standards was used for calibration. Analyses of secondary standards (KK1, BCR2 and Diopside) were repeated each day to identify any instrumental drift, for which no corrections were necessary. Precision on major elements was assessed from the reproducibility (2σ) of repeat analyses of standard materials: <1% for FeO, <2% for SiO_2, Al_2O_3, CaO, <3% for MgO, TiO_2 and <5% for K_2O. Counting times were 10 s for Na, Si, Al, K and Ca, and 30 s for Mg, S, P, Ti, Fe and Mn, over a total analysis time of 60 s. Analyses that were contaminated by crystal phases were excluded. All compositions are shown as oxides normalised to anhydrous composition (see Table 3). Multivariate analysis in the form of Principal Component Analysis (PCA) was applied to standardised (z-scored) matrix glass compositions using RStudio statistical software (*prcomp* function) to explore and quantify the variance in the dataset. PCA is a statistical procedure for dimensionality reduction: for a set of samples, the process reduces *n* independent variables to *n-1* principal components made up of weighted combinations of the original variables (loadings). Generally, between 2 and 4 principal components account for most of the variance within a dataset, therefore PCA plots of PC1 vs PC2 provide a way to visualise the relationships between samples based on multiple characteristics. Na_2O, MnO, P_2O_3 and SO_2 were excluded from the PCA input matrix due to the larger uncertainties on these minor/volatile elements. Rhyolitic glass compositions in L6-A were excluded from the PCA analysis, as they dominated the variance and therefore masked differences in basaltic glass composition.

4. RESULTS

4.1 Geomorphological setting

The distribution of glacial and periglacial features suggests the existence of several stages during the long-term deglaciation of this peninsula. We identified three moraine systems in Barton Peninsula (Fig. 3):

(1) The Outer moraine complex (I) is formed by the lateral moraines of the tide-water glacier that occupied Marian Cove – distributed on the raised beach at +9 m asl –, as well as the frontal moraine ridges at the SE margin of the peninsula at elevations between 80 and 150 m asl. Lakes L5, L6 and L11 are located ahead of this moraine complex on relatively flat surfaces associated with to the Upper (L11) and the Middle (L5 and L6) marine platforms.

(2) The Intermediate moraine complex (II) consists of frontal and lateral moraines distributed in two areas: (a) along the SE fringe of the peninsula, frontal moraines of the ice dome are located between 140 and 145 m asl, and (b) in the northern and western areas, with lateral and frontal moraines located ca. 150 m downslope from the small glaciers formed in a cirque shaped between the Sejong (255 m asl) and Baekdu (290 m asl) peaks (Araon Valley). Lake L12 is dammed by this moraine complex.

(3) The Inner moraine complex (III) is formed by small frontal moraines located in the glacial cirques, as well as on the edge of the present-day dome glacier. Whereas the first sets of moraines are distributed at elevations 110-150 m asl (W) and 150-175 m asl (E), the others are located below the raised beach of +3 m asl, thus being reshaped by present-day marine processes. Lake L13, located ca. 30 m from the present-day glacier front, is dammed by this moraine system.

Figure 3

4.2 Lacustrine sedimentary sequences

The complete sedimentary sequence was collected from lakes L6, L11, L13 and possibly in L12, but not in lake L5 (Fig. 4) where we could not reach the lowermost sediments. A similar situation occurred in a number of other lakes across Barton Peninsula, where the presence of gravels precluded the recovery of underlying sediments. The lake sediment cores from Barton Peninsula showed very different characteristics in terms of of lithological composition and colouration (Fig. 4):

Figure 4

Lake L5 record

A 43 cm long core recovered from Lake L5 contained inorganic sediments:

- Unit 1 (43-29 cm) was composed of centimetric, faintly-banded yellow, brown, and red sediments with some gravels (Ø < 5 mm). A bulk sediment sample from the depth 42 cm was dated at 2890 ± 55 cal yr BP.
- Unit 2 (29-5 cm) included alternating three cm-thick black tephra layers and yellow silty layers. These tephra layers were present at 20.2-21.5, 17-18.5 (L5-A), and 15-15.5 (L5-B) cm depth.
- Unit 3 (5-0 cm) showed alternating mm-scale black and yellow silty layers. A dark, coarse-grained tephra layer was found at the base of the unit (4-4.5 cm; L5-C). The base of this unit was dated at 1340 ± 45 cal yr BP.

Lake L6 record

A 98 cm long core collected from Lake L6 contained three lithological units:

- Unit 1 (98-65 cm) contained alternating cm-thick layers of light and dark grey silty sediments. A coarse-grained dark tephra layer of variable thickness between 5 and 10 mm was found at a depth 86-87 cm (tephra L6-A). A bulk sediment sample from the depth 94 cm was dated at 7940 ± 45 cal yr BP.
- Unit 2 (65-27 cm) was composed of massive dark brown silts, with dark sandy layers at 34-36 and 51-53 cm that are interpreted as tephra layers.
- Unit 3 (27-0 cm) was made up of centimetric-scale light and dark banded coarse-grained sediments. A 2 cm-thick coarse-grained dark tephra layer was found at the base of the unit (25-27 cm depth; L6-B), overlain by 3 cm of fine, dark, sandy, ash-rich sediment. A 5 mm fine-grained dark tephra horizon with a sharp base is present at 16–16.5 cm depth (L6-C).

Lake L11 record

A 24 cm long core retrieved from Lake L11 showed major changes in terms of colour and texture properties:

- Unit 1 (24-11 cm) was composed of sandy-silty sediments with some gravels at the base (Ø < 5 mm). The ^{14}C sample of bulk sediment from the base of the unit returned an age of 3720 ± 110 cal yr BP.
- Unit 2 (11-4.5 cm) contained coarse-grained sediments, with gravel up to 20 mm in a sandy matrix. Some moss remnants were present in the upper part of this unit.
- Unit 3 (4.5-0 cm) consisted of light brown organic-rich silty sediments.

Lake L12 record

A 37 cm long core was collected from Lake L12, which displayed a centimeter-scale alternation of light and dark grey silty clays. This sequence had a pronounced dip (up to 40º) at the bottom, progressively decreasing towards the top of the core. A number of moss layers were interbedded in this section. The moss layer near the core base provided a calibrated age of 2440 ± 80 cal yr BP. In the uppermost 13 cm of the core, several mm- to cm-thick dark layers, interpreted as tephra deposits, were present.

Lake L13 record

A 30 cm long core was collected from Lake L13 and contained four different lithological units:

- Unit 1 (30-27 cm) was composed of gravels (Ø < 30 mm) embedded in a sandy matrix.
- Unit 2 (27-17 cm) was made up of dark grey massive silty-clays with some scattered gravels (Ø < 5 mm). A bulk sediment sample at 21 cm depth returned an age of 4660 ± 90 cal yr BP.
- Unit 3 (17-10 cm) was composed of dark grey fine sands. An irregular-shaped 1 cm thick tephra layer constituted the base of this unit (L13-A).
- Unit 4 (10-0 cm) included a centimeter-scale alternation of dark and light grey silty clays and fine sands. Two tephra layers were observed at 9-10 cm (L13-B) and 4.5-8 cm (L13-C) depth.

4.3 Tephra layers

Tephra layers from the two best preserved lake cores (L5 and L6) were selected for geochemical analyses (Fig. 4). Average major element glass compositions from six sampled tephra layers are presented in Table 3 (additional data are presented in Table A, supplementary material). The analysed tephras were generally basaltic to basaltic andesite in glass composition (50–58 wt% SiO_2; Fig. 5). However, L6-A was compositionally

bimodal; although most tephra grains comprised basaltic glasses, a minor population were characterised by higher silica glasses of rhyolitic composition (52–55 and 72–73 wt% SiO_2, respectively).

Considered together, basaltic glasses from all layers reproduced trends that mirror expected liquid lines of descent for mafic mineral crystallisation (i.e., olivine, plagioclase and clinopyroxene; Fig. 5). L6-A and L5-A were characterised by relatively homogeneous glass compositions with small standard deviations, whilst stratigraphically higher tephra layers exhibited much greater variance. This increased variance may reflect true magmatic geochemical processes at source, variable degrees of post-depositional chemical alteration, or reworking of multiple tephra deposits. L6-A, L6-C, L5-A, L5-B and L5-C occupied overlapping compositional fields with respect to most major elements. However, L6-B was compositionally distinct outside of analytical uncertainty, comprising matrix glasses enriched in incompatible elements (e.g., SiO_2 and K_2O) indicative of a more evolved melt composition. Importantly for the purposes of stratigraphic correlation, L6-B can be distinguished entirely from other samples by FeO and TiO_2, which likely reflects the appearance of magnetite in the crystallising assemblage (not observed in other samples).

Multivariate PCA analysis demonstrates that 93% of the total variance (including published data from Byers Peninsula, see Discussion) within the dataset can be accounted for by the first two principal components (PC1 and PC2; Fig. 6). PCA loadings are detailed in Table B, supplementary information. Although PC1 contains relatively even contributions from all oxides, it is dominated by K_2O (negative) and CaO, MgO (positive). PC2 is dominated by FeO, TiO_2 (negative) and SiO_2 (positive). When all tephra samples are plotted as a function of the first two principal components, L6-B is distinct from other Barton tephras in the PC2 direction, with L6-B glasses statistically lower in FeO and TiO_2, and higher in SiO_2. PCA statistics are, therefore, in good agreement with the qualitative observations described above.

Table 3

Figure 5

Figure 6

5- DISCUSSION

5.1 Deglaciation timescale

Most of the glaciers on the Antarctic Peninsula have retreated significantly during the last century (Davies, Carrivick, Glasser, Hambrey, & Smellie, 2012; Seehaus, Cook, Silva, & Braun, 2018). King George Island, and, consequently, Barton Peninsula, is no exception with the total glaciated area having declined during the last several decades (Simoes, Rosa, Czapela, Vieira, & Simoes, 2015). This pattern must be framed within the long-term pattern of glacial retreat in the Antarctic Peninsula region detected since the mid-20th century in response to one of the fastest rates of warming recorded on Earth, with temperature increases of ca. 0.5 °C/decade (Turner et al. 2005). However, there is evidence that glacier retreat may have decelerated during recent years in the SSI (Navarro et al. 2013; Oliva et al. 2017a).

During the Last Glacial, the SSI were covered by an extensive ice cap connected with the Antarctic Peninsula that began to shrink as temperatures started increasing at ca. 18 ky (Stenni et al. 2011), and by 15 ky the ice cap encircling these islands became isolated from the rest of the continent (Ingólfsson et al. 2003; Hall, 2009; Ó Cofaigh et al. 2014). On King George Island, the Collins Glacier thinned gradually and the highest peaks protruded the ice as nunataks. Topographic maxima in the Barton Peninsula became ice-free between 11.9 and 15.5 ky, as inferred from surface exposure dating (Seong et al. 2009). Glaciomarine sediments from Maxwell Bay and Marian Cove also confirm the deglaciation of the bay between 14 and 17 cal ky BP (Yoon et al. 1997; Milliken et al. 2009; Simms et al. 2011). This glacial thinning was accompanied by a gradual retreat inland of the ice caps during the Early Holocene 10.1 and 8.2 cal ky BP (Bentley et al. 2009; Milliken et al. 2009; Shevenell, Ingalls, Domack, & Kelly, 2011), when the continent recorded the highest temperatures of the Holocene, reaching values ca. 6 ºC higher than those recorded during the LGM (Mulvaney et al. 2012).

According to the lithological column of the studied lakes, there are no evidences of hiatuses or other sedimentological features between the oldest lacustrine sediments and the lake basement rocks, like incipient soils, that might indicate long time exposure. Therefore, lakes started to be present at Barton Peninsula just after

the glacier retreat began. The basal radiocarbon ages from Barton Peninsula lakes suggest that land surfaces began to deglaciate roughly by 8 cal ky BP and proceeded from the southeast to the north. Lakes L5 and L6 are located on a marine platform ca. 2 km from the current front of the Collins Glacier. These lakes are in similar topographic environments, filling depressions distributed above a cliff falling to a sequence of marine terraces. The lakes are separated by a distance of only 700 m, and yet the radiocarbon dates of the basal sediments in each lake indicate significant chronological differences: L5 showed an age of 2.9 cal ky BP, while L6 was formed at 7.9 cal ky BP. As we did not reach the oldest sediments in L5, which showed high compaction near the bottom of the core, disabling the penetration of the corer, the L5 radiocarbon age cannot be used as a marker for the deglaciation chronology of this site. The significantly older age in Lake L6 is similar to coastal lakes cored from nearby Fildes Peninsula on King George Island (Watcham et al. 2011) or in other lake records of the SSI, such as in Byers Peninsula from Livingston Island (Toro et al. 2013; Oliva et al. 2016). The basal ^{14}C date of Lake L6 suggests that the southern area was the first coastal environment of Barton Peninsula to become ice-free. Along the northern coast of the peninsula, the existence of several exposure ages between 1 and 2 ky suggests that this area was only deglaciated during the Late Holocene (Fig. 7; Seong et al. 2009). The northwards retreat of the Collins Glacier during the Early Holocene was accompanied by a shrinking of the ice cap, shown by the cosmogenic age of 7.6 ky that suggests the deglaciation of the high central plateau of Barton Peninsula during this time (Seong et al. 2009).

Figure 7

The relative homogeneity of cosmogenic ages below 150 m asl around the central plateau (ranging between 3.8 and 7.6 ky; Seong et al. 2009) suggests that the Collins Glacier was generally stable during the Mid-Holocene, without major advances or retreats in Barton Peninsula. On Byers Peninsula, a period with relative glacial stability or with minor glacier advances and retreats was also recorded after 7.5 cal ky BP (Oliva et al. 2016). This glacial stability is also supported by the presence of Lake L11. The basal sediments of this lake reported an age of 3.7 cal ky BP, which is indicative of a minimum age for the formation of the moraine system located next to it. The similarity of this date with that obtained by cosmogenic dating of polished bedrock (3.8 ky) strongly supports a period of glacial retreat starting at this time. The Mid-Late Holocene deglaciation also led

to the appearance of new land surfaces in the SSI resulting both from glacial retreat and the emergence of former marine terraces due to glacio-isostatic uplift. The reduction in glaciated area in the SSI caused an uplift of ca. 14 m in Barton Peninsula (Fretwell et al. 2010), which implies that the lowlands and coastal lagoons of this peninsula only appeared over the last few millennia.

The other two lakes (i.e., L12 and L13) are located in a glacial valley that still contains a small cirque glacier in the upper part of the catchment. The modern glacier front is situated at 110 m asl, where it forms a small moraine ridge. The retreat of the glacier has formed several moraines, some of which dam lakes and ponds, such as L12 and L13. Lake L12 is located in a small glacial depression at 102 m asl, enclosed by the most distal moraine, and L13 shows the same geomorphological pattern at a slightly higher elevation, at 110 m asl. However, the basal sediments in both lakes show inverted ages relative to those expected: while L13, in contact with the glacier front, reported an age of 4.7 cal ky BP, the oldest sediments in L12 yielded 2.4 cal ky BP. One possible explanation is that due to its proximity to the glacier front, lake L13 continues to be contaminated with old carbon released from the glacier. The radiocarbon age may thus not reflect the true age of deglaciation at this site. Many Antarctic lacustrine records report radiocarbon ages that may have been influenced by old carbon stored in several sources, such as permafrost, glacial ice or ornithogenic soils (Hendy & Hall, 2006; Vonk et al. 2015). The contamination of samples with radiocarbon-depleted material (both for bulk sediment and organic fragments) is an under-investigated problem in paleoenvironmental studies from polar regions that can lead to large uncertainties on ages, and at worse, highly erroneous results (Antoniades et al. 2018; Píšková et al., 2019). This is a widespread problem in permafrost regions due to the good preservation of organic materials (Schuur et al. 2009) as well in glacier forelands with old ancient carbon being released by the melting glacier (Hågvar & Ohlson, 2013, Hood, Battin, Fellman, O'Neel, & Spencer, 2015). Alternately, L12 simply may not have formed until a later stage of landscape evolution or we may have not reached the base of the sedimentary sequence. Assuming a minimum age of 2.4 cal ky BP for the base of L12 and considering that the present-day glacier front is located only 150 m from this lake (Fig. 8), our results suggest that the glacier has not experienced substantial advances during the Late Holocene, with only a minor glacial advance or a phase of stabilization for the last 2.4 cal ky BP that formed the moraine enclosing the lake L13. This glacier stabilization during the Late

Holocene has also been reported for other ice-free environments in the SSI, such as Byers Peninsula (Oliva et al. 2016).

Figure 8

5.2 Tephra layers chronological markers

Matrix glass compositions from all sampled tephra layers plot within the compositional field of Deception Island volcano (located 125 km SE of Barton Peninsula) and distinct from those of other local volcanic centres (Fig. 9). Deception Island is, therefore, the most likely source of the volcanic material. Deception Island is a composite stratovolcano comprising a mostly submerged caldera ca. 10 km in diameter, and during its history has erupted a broad spectrum of magma compositions from basalt to dacite (Smellie, 2001; Martí, Geyer, & Aguirre-Díaz, 2013). This volcano has been the primary source of Holocene tephra deposits to the SSI throughout the Holocene (Kraus, Kurbatov, & Yates, 2013), with tephra layers geochemically consistent with Deception Island documented in lacustrine sediments from Byers Peninsula (Björck, Sandgren, & Zale, 1991; Hodgson, Dyson, Jones, & Smellie, 1998; Toro et al. 2013; Liu et al. 2016; Antoniades et al. 2018) and King George Island (Lee et al. 2007; Roberts et al. 2017), and marine sediments from the Scotia Sea (Moreton & Smellie, 1998) and Bransfield Basins (Fretzdorff & Smellie, 2002).

Figure 9

In Byers Peninsula (Livingston Island, SSI), three major tephra horizons – T1 (1890 ± 140 cal yr BP), T2 (2370 ± 100 cal yr BP), and T3 (3980 ± 125 cal yr BP) – were correlated between three lakes based on their geochemical and textural properties, and their ages were constrained using AMS radiocarbon dates (Toro et al. 2013; Liu et al. 2016; Antoniades et al. 2018). The T3 tephra deposit is geochemically distinct, with glass compositions more depleted in compatible elements indicative of mafic mineral fractionation (e.g. Fe, Mg and Ti). In the longest Byers Peninsula core (Escondido Lake), two additional tephra layers older than the T3 isochron were found to be geochemically similar to the younger T1 and T2 compositions, thereby constraining T3 as a geochemically distinct marker horizon (Liu et al. 2016). Geochemical two-component plots and

multivariate PCA show that whilst tephra layers L6-A, L6-C, L5-A, L5-B, and L5-C are most closely related to the T1 and T2 compositions (particularly in PC2), tephra L6-B is statistically similar to the T3 tephra in both PC1 and PC2 (Figs. 5, 6). The centroids for L6-B and T3 plot closely in the same quadrant, indicating that the two sample populations share overlapping characteristics in multiple variables (oxides).

Tephra layers in other lake sedimentary sequences from King George Island (Fildes Peninsula; Fig. 1) provide additional temporal constraints. The oldest tephras – referred to as D and E in Lee et al. (2007) – are older than ca. 5 cal ky BP and exhibit characteristic bimodal compositions; they may therefore be correlative of the oldest Barton tephra layer L6-A. A major primary tephra deposit in the Fildes Peninsula sedimentary sequences is overlain by massive gravity-flow deposits similar to those documented in association with the T3 tephra (Antoniades et al. 2018), and its base is dated at 4.9 cal ky BP (Lee et al. 2007). This tephra deposit is geochemically and sedimentologically similar to L6-B and T3, and therefore supports the relative chronology despite the discrepancy in absolute age. As discussed above, this may be related to the presence of old organic carbon stored in lake sediments from a catchment affected by changing permafrost conditions during the Holocene.

The presence of the T3 tephra deposit in lake L6 but not in L5 would imply that the base of L5 is not older than the well-constrained age of 3980 ± 125 cal yr BP of T3 in the SSI and neighbouring areas (Antoniades et al. 2018), which is consistent with the younger basal radiocarbon date for L5 of 2.9 cal ky BP (compared to 7.9 cal ky BP for L6). The inferred ages of the Barton Peninsula tephras, based on geochemical comparison to other dated tephra sequences, support the chronological framework from independent radiocarbon dates presented in this study.

CONCLUSIONS

Lake sediment records from Barton Peninsula provide information of the environmental evolution in King George Island during the Holocene. The basal radiocarbon dates of sedimentary sequences from five lakes of the western part of Barton Peninsula offer a more accurate chronology on the Holocene deglaciation of this ice-

free area, although surface exposure dating suggest that glacial retreat in Barton Peninsula started several millennia ago.

During the Last Glacial, the SSI were covered by an ice sheet connected with the Antarctic Peninsula region, which started thinning between 15 and 20 ky and became isolated encircling the SSI. The thinning of the Collins Glacier accompanied marginal retreat, which exposed the lowest coastal environments along the southern fringe of the peninsula at ca. 8 cal ky BP. The ice cap was relatively stable during the Late Holocene, but retreated northwards after 3.7 cal ky BP. This glacial shrinking confined some glaciers within valleys, where they are still present. This is the case for a small glacial valley on Barton Peninsula where lake sediments reveal glacial stability during the Late Holocene, with no major advances, during, at least, the last 2.4 cal ky BP. The presence of small moraines ridges indicates two minor glacial advances and/or phases of glacier stabilization during these millennia.

Deception Island volcano has been identified as the dominant source for the volcanic event horizons recorded in the sediments of Barton Peninsula. Visible tephra layers within two lake sequences record persistent eruptive activity during the Holocene. Although matrix glass compositions are relatively homogeneous through time, a key marker horizon (L6-B) has been identified based on geochemically properties to a large eruption (T3) documented in lacustrine and marine sediment records throughout the northern AP region (Antoniades et al. 2018). The independent age constraints provided by the stratigraphic position of this major eruption are consistent with the sequence of events inferred from basal lake sediments of Barton Peninsula. Together, these multiple lines of evidence provide compelling support for the chronological deglaciation framework presented in this study.

ACKNOWLEDGEMENTS

The authors are grateful to the Portuguese Polar Program (PROPOLAR), the Korea Polar Research Institute (KOPRI) and the Chilean Antarctic Institute (INACH) for providing logistic support for the field work. Marc Oliva is supported by the Ramón y Cajal Program (RYC-2015-17597) and the Research Group ANTALP (Antarctic, Arctic, Alpine Environments; 2017-SGR-1102) funded by the Government of Catalonia through the AGAUR agency. The work complements the research topics examined in the PALEOGREEN (CTM2017-87976-P) and CRONOANTAR (CTM2016-77878-P) projects of the Ministry of Economy, Industry and Competitiveness, Spain, and the projects *Analysis of nunataks of the Antarctic Peninsula as multiproxy data sources on environmental change and climate dynamics* - NUNANTAR (02/SAICT/2017 - 32002) and *Holocene environments in Barton Peninsula (South Shetland Islands, Antarctica)* funded by the Fundação para a Ciência e a Tecnologia, Portugal. We also thank João Agrela for the support during field work.

REFERENCES

Antoniades, D., Giralt, S., Geyer, Álvarez-Valero, A. M., Pla-Rabes, S., Granados, I., Liu, E. J., Toro, M., Smellie, J., & Oliva, M. (2018). The timing and widespread effects of the largest Holocene volcanic eruption in Antarctica. *Scientific Reports, 8,* 17279.

Bentley, M. J., Hodgson, D. A., Smith, J. A., O Cofaigh, C., Domack, E. W., Larter, R. D., Roberts, S. J., Brachfeld, S., Leventer, A., Hjort, C., Hillenbrand, C. D., & Evans, J. (2009). Mechanisms of Holocene paleoenvironmental change in the Antarctic Peninsula region. *The Holocene, 19,* 51–69.

Bentley, M. J., Cofaigh, C. O., Anderson, J. B., Conway, H., Davies, B., Graham, A. G. C., Hillenbrand. C. D., Hodgson, D. A., Jamieson, S. S. R., Larter, R. D., Mackintosh, A., Smith, J. A., Verleyen, E., Ackert, R. P., Bart, P. J., Berg, S., Brunstein, D., Canals, M., Colhoun, E. A., Crosta, X., Dickens, W. A., Domack, E., Dowdeswell, J. A., Dunbar, R., Ehrmann, W., Evans, J., Favier, V., Fink, D., Fogwill, C. J., Glasser, N. F., Gohl, K., Golledge, N. R., Goodwin, I., Gore, D. B., Greenwood, S. L., Hall, B. L., Hall, K., Hedding, D. W., Hein, A. S., Hocking, E. P., Jakobsson, M., Johnson, J. S., Jomelli, V., Jones, R. S., Klages, J. P., Kristoffersen, Y., Kuhn, G., Leventer, A., Licht, K., Lilly, K., Lindow, J., Livingstone, S. J., Masse, G., McGlone, M. S., McKay, R. M., Melles, M., Miura, H., Mulvaney, R., Nel, W., Nitsche, F. O., O'Brien, P. E., Post, A. L., Roberts, S. J., Saunders, K. M., Selkirk, P. M., Simms, A. R., Spiegel, C., Stolldorf, T. D., Sugden, D. E., Van

der Putten, N., van Ommen, T., Verfaillie, D., Vyverman, W., Wagner, B., White, D. A., Witus, A. E., & Zwartz, D. (2014). A community-based geological reconstruction of Antarctic Ice Sheet deglaciation since the Last Glacial Maximum. *Quaternary Science Reviews, 100,* 1–9.

Björck, S., Sandgren, P., & Zale, R. (1991). Late Holocene tephrochronology of the northern Antarctic Peninsula. *Quaternary Research, 36,* 322–328.

Bockheim, J., Vieira, G., Ramos, M., López-Martínez, J., Serrano, E., Guglielmin, M., Wilhelm, K., & Nieuwendam, A. (2013). Climate warming and permafrost dynamics in the Antarctic Peninsula region. *Global Planetary Change, 100*, 215–223.

Correia, A., Oliva, M., & Ruiz-Fernández, J. (2017). Evaluation of frozen ground conditions along a coastal topographic gradient at Byers Peninsula (Livingston Island, Antarctica) by geophysical and geoecological methods. *Catena, 149 (2)*, 529–537.

Davies, R. E. S. (1982). The geology of the Marian Cove area, King George Island, and a Tertiary age for its supposed Jurassic volcanic rocks. *British Antarctic Survey Bulletin, 51*, 294–296.

Davies, B. J., Carrivick, J. L., Glasser, N. F., Hambrey, M. J., & Smellie, J. L. (2012). Variable glacier response to atmospheric warming, northern Antarctic Peninsula, 1988-2009. *The Cryosphere, 6,* 1031–1048.

Denton, G. H., Anderson, R. F., Toggweiler, J. R., Edwards, R. L., Schaefer, J. M., & Putnam, A. E. (2010). The Last Glacial Termination. *Science, 328,* 1652–1656.

Fretwell, P. T., Hodgson, D. A., Watcham, E. P., Bentley, M. J., & Roberts, S. J. (2010). Holocene isostatic uplift of the South Shetland Islands, Antarctic Peninsula, modelled from raised beaches. *Quaternary Science Reviews, 29*, 1880–1893.

Fretzdorff, S., & Smellie, J. L. (2002). Electron microprobe characterization of ash layers in sediments from the central Bransfield basin (Antarctic Peninsula): evidence for at least two volcanic sources. *Antarctic Science*, *14*, 412–421.

Hågvar, S., & Ohlson, M. (2013). Ancient carbon from a melting glacier gives high ^{14}C age in living pioneer invertebrates. *Scientific Reports, 3,* 2820.

Hall, B. L. (2009). Holocene glacial history of Antarctica and sub-Antarctic Islands. *Quaternary Science Reviews, 28,* 2213–2230.

Hendy, C. H., & Hall, B. L. (2006). The radiocarbon reservoir effect in proglacial lakes: examples from Antarctica. *Earth and Planetary Science Letters, 241*, 413–421.

Hodgson, D. A., Dyson, C. L., Jones, V. J. & Smellie, J. L. (1998). Tephra analysis of sediments from Midge Lake (South Shetland Islands) and Sombre Lake (South Orkney Islands), Antarctica. *Antarctic Science, 10*, 13–20.

Hrbáček, F., Vieira, G., Oliva, M., Balks, M., Guglielmin, M., de Pablo, M. A., Molina, A., Ramos, M., Goyanes, G., Meiklejohn, I., Abramov, A., Demidov, N., Fedorov-Davydov, D., Lupachev, A., Rivkina, E., Láska, K., Kňažková, M., Nývlt, D., Raffi, R., Strelin, J., Sone, T., Fukui, K., Dolgikh, A., Zazovskaya, E., Mergelov, N., Osokin, N., & Miamin, V. (2018). Active layer monitoring in Antarctica (CALM-S): results from 2006-2015 and new perspectives. *Polar Geography*, doi: 10.1080/1088937X.2017.1420105.

Hood, E., Battin, T. J., Fellman, J., O'Neel, S., & Spencer, R. G. M. (2015). Storage and release of organic carbon from glaciers and ice sheets. *Nature Geoscience, 8*, 91–96.

Ingólfsson, O., Hjort, C., & Humlum, O. (2003). Glacial and climate history of the Antarctic Peninsula since the Last Glacial Maximum. *Arctic, Antarctic, and Alpine Research, 35 (2),* 175–186.

Kraus, S., Kurbatov, A., & Yates, M. (2013). Geochemical signatures of tephras from Quaternary Antarctic Peninsula volcanoes. *Andean Geology, 40,* 1–40.

Lee, J. I., Yur, S. D., Yoo, C. M., Yeo, J. P., Kim, H., Choe, M. Y., Nam, S. H., Kim, Y., Park, B. K., Zheng, X., & López-Martínez, J. (2002). *Geological Map of Barton and Weaver peninsulas, King George Island, Antarctica, scale. 1:10,000*. Korea Ocean Research and Development Institute. Seoul.

Lee, Y. I., Lim, H. S., Yoon, H. I. & Tatur, A. (2007). Characteristics of tephra in Holocene lake sediments on King George Island, West Antarctica: implications for deglaciation and paleoenvironment. *Quaternary Science Reviews, 26 (25–28*), 3167–3178.

Liu, E. J., Oliva, M., Antoniades, D., Giralt, S., Granados, I., Pla-Rabes, S., Toro, M., & Geyer, A. (2016). Expanding the tephrostratigraphical framework for the South Shetland Islands, Antarctica, by combining compositional and textural tephra characterisation. *Sedimentary Geology, 340,* 49–61.

López-Martínez, J., Serrano, E., & Lee, J. I. (2002). *Geomorphological map of Barton and Weaver peninsulas, King George Island, Antarctica, scale: 1:10.000*. Korea Ocean Research and Development Institute. Seoul.

López-Martínez, J., Serrano, E., Schmid, T., Mink, S., & Linés, C. (2012). Periglacial processes and landforms distribution in the South Shetland Islands (northern Antarctic Peninsula region). *Geomorphology, 155–156*, 62–79.

Martí, J., Geyer, A., & Aguirre-Díaz, G. (2013). Origin and evolution of the Deception Island caldera (South Shetland Islands, Antarctica). *Bulletin of Volcanology, 75*, 1–18.

Milliken, K. T., Anderson, J. B., Wellner, J. S., Bohaty, S. M., & Manley, P. L. (2009). High-resolution Holocene climate record from Maxwell Bay, South Shetland Islands, Antarctica. *Bulletin of the Geological Society of America, 121,* 1711–1725.

Moreton, S .G., & Smellie, J. L. (1998). Identification and correlation of distal tephra layers in deep-sea sediment cores, Scotia Sea, Antarctica. *Annals of Glaciology, 27,* 285–289.

Mulvaney, R., Abram, N. J., Hindmarsh, R. C., Arrowsmith, C., Fleet, L., Triest, J., Sime, L. C., Alemany, O., & Foord, S. (2012). Recent Antarctic Peninsula warming relative to Holocene climate and ice-shelf history. *Nature, 489,* 141–144.

Navarro, F., Jonsell, U., Corcuera, M. I., & Martín-Español, A. (2013). Decelerated mass loss of Hurd and Johnsons Glaciers, Livingston Island, Antarctic Peninsula. *Journal of Glaciology, 59 (213),* 115–128.

Ó Cofaigh, C., Davies, B. J., Livingstone, S. J., Smith, J. A., Johnson, J. S., Hocking, E. P., Hodgson, D. A., Anderson, J. B., Bentley, M. J., Canals, M., Domack, E., Dowdeswell, J. A., Evans, J., Glasser, N. F., Hillenbrand, C. D., Larter, R. D., Roberts, S. J., & Simms, A. R. (2014). Reconstruction of ice-sheet changes in the Antarctic Peninsula since the Last Glacial Maximum. *Quaternary Science Reviews, 100,* 87–110.

Oliva, M., & Ruiz-Fernández, J. (2015). Coupling patterns between paraglacial and permafrost degradation responses in Antarctica. *Earth Surface Processes and Landforms, 40 (9),* 1227–1238.

Oliva, M., Antoniades, D., Giralt, S., Granados, I., Pla-Rabes, S., Toro, M., Sanjurjo, J., Liu, E. J., & Vieira, G. (2016). The Holocene deglaciation of the Byers Peninsula (Livingston Island, Antarctica) based on the dating of lake sedimentary records. *Geomorphology, 261,* 89–102.

Oliva, M., Navarro, F. J., Hrbáček, F., Hernández, A., Nývlt, D., Pereira, P., Ruiz-Fernández, J., & Trigo, R. (2017a). Recent regional cooling of the Antarctic Peninsula and its impacts on the cryosphere. *Science of the Total Environment, 580,* 210–223.

Oliva, M., Hrbáček, F., Ruiz-Fernández, J., De Pablo, M. A., Vieira, G., Ramos, M., & Antoniades, D. (2017b). Active layer dynamics in three topographically distinct lake catchments in Byers Peninsula (Livingston Island, Antarctica). *Catena, 149 (2)*, 548–559.

Osmanoğlu, B., Braun, M., Hock, R., & Navarro, F .J. (2013). Surface velocity and ice discharge of the ice cap on King George Island, Antarctica. *Annals of Glaciology, 54(63),* 111–119.

Píšková, A., Roman, M., Bulínová, M., Pokorný, M., Sanderson, D., Cresswell, A., Lirio, J.M., Coria, S.H., Nedbalová, L., Lami, A., Musazzi, S., Van de Vijver, B., Nývlt, D., & Kopalová, K. (2019). Late-Holocene palaeoenvironmental changes at Lake Esmeralda (Vega Island, Antarctic Peninsula) based on a multi-proxy analysis of laminated lake sediment. The Holocene, doi: 10.1177/0959683619838033.

Reimer, P. J., Bard, E., Bayliss, A., Beck, J. W., Blackwell, P. G., Bronk Ramsey, C., Buck, C. E., Cheng, H., Edwards, R. L., Friedrich, M., Grootes, P. M., Guilderson, T. P., Haflidason, H., Hajdas, I., Hatté, C., Heaton, T. J., Hoffmann, D. L., Hogg, A., Hughen, K. A., Kaiser, K. F., Kromer, B., Manning, S. W., Niu, M., Reimer, R. W., Richards, D. A., Scott, E. M., Southon, J. R., Staff, R. A., Turney, C. S. M., & van der Plicht, J. (2013). IntCal13 and Marine13 radiocarbon age calibration curves 0-50,000 years cal BP. *Radiocarbon, 55 (4),* 1869–1887.

Roberts, S. J., Monien, P., Foster, L. C., Loftfield, J., Hocking, E. P., Schnetger, B., Pearson, E. J., Juggins, S., Fretwell, P., Ireland, L., Ochyra, R., Haworth, A. R., Allen, C. S., Moreton, S. G., Davies, S. J., Brumsack, H. J., Bentley, M. J., & Hodgson, D. A. (2017). Past penguin colony responses to explosive volcanism on the Antarctic Peninsula. *Nature Communications, 8*, 14914.

Ruiz-Fernández, J., & Oliva, M. (2016). Relative palaeoenvironmental adjustments following deglaciation of the Byers Peninsula (Livingston Island, Antarctica). *Arctic, Antarctic and Alpine Research, 48 (2),* 345–359.

Ruiz-Fernández, J., Oliva, M., & García-Hernández, C. (2017). Topographic and geomorphologic controls on the distribution of vegetable formations in Elephant Point (Livingston Island, Maritime Antarctica). *Science of the Total Environment, 587–588,* 340–349.

Ruiz-Fernández, J., Oliva, M., Nývlt, D., Cannone, N., García-Hernández, C., Guglielmin, M., Hrbáček, F., Roman, M., Fernández, S., & López-Martínez, J. (2019). Paraglacial response since the Last Glacial Maximum in the Antarctic Peninsula region. *Earth-Science Reviews, 192,* 379–402.

Schuur, E. A., Vogel, J. G., Crummer, K. G., Lee, H., Sickman, J. O., & Osterkamp, T. E. (2009). The effect of permafrost thaw on old carbon release and net carbon exchange from tundra. *Nature, 459,* 556–559.

Seehaus, T., Cook, A. J., Silva, A. B., & Braun, M. (2018). Changes in glacier dynamics in the northern Antarctic Peninsula since 1985. *The Cryosphere, 12*, 577–594.

Seong, Y. B., Owen, L. A., Lim, H. S., Yoon, H. I., Kim, Y., Lee, Y. I. & Caffee, M. W. (2009). Rate of late Quaternary ice-cap thinning on King George Island, South Shetland Islands, West Antarctica, defined by cosmogenic 36Cl surface exposure dating. *Boreas, 38,* 207–213.

Serrano, E., & López-Martínez, J. (2004). Morfogénesis periglaciar y deglaciación en las penínsulas Barton y Weaver (islas Shetland del Sur, Antártida). *Boletín Real Sociedad Española de Historia Natural, 99 (1-4),* 131–140.

Shevenell, A. E., Ingalls, A. E., Domack, E. W., & Kelly, C. (2011). Holocene Southern Ocean surface temperature variability west of the Antarctic Peninsula. *Nature, 470,* 250–254.

Simms, A. R., Milliken, K. T., Anderson, J. B., & Wellner, J. S. (2011). The marine record of deglaciation of the South Shetland Islands, Antarctica since the Last Glacial Maximum. *Quaternary Science Reviews, 30,* 1583–1601.

Simoes, C. L., Rosa, K. K., Czapela, F. F., Vieira, R., & Simoes, J. C. (2015). Collins glacier retreat process and regional climatic variations, King George Island, Antarctica. *Geographical Review, 105,* 462–471.

Smellie, J. L. (2001). Lithostratigraphy and volcanic evolution of Deception Island, South Shetland Islands. *Antarctic Science, 13*, 188–209.

Stenni, B., Buiron, D., Frezzoti, M., Albani, S., Barbante, C., Bard, E., Barnola, J. M., Baroni, M., Baumgartner, M., Bonazza, M., Capron, E., Castellano, E., Chappellaz, J., Delmonte, B., Falourd, S., Genoni, L., Iacumin, P., Jouzel, J., Kipfstuhl, S., Landais, A., Lemieux-Dudon, B., Maggi, V., Masson-Delmotte, V., Mazzola, C., Minster, B., Montagnat, M., Mulvaney, R., Narcisi, B., Oerter, H., Parrenin, F., Petit, J. R., Ritz, C., Scarchilli, C., Schilt, A., Schüpbach, S., Schwander, J., Selmo, E., Severi, M., Stocker, T. F., & Udisti, R. (2011). Expression of the bipolar see-saw in Antarctic climate records during the last deglaciation. *Nature Geoscience, 4,* 46–49.

Toro, M., Granados, I., Pla, S., Giralt, S., Antoniades, D., Galán, L., Martínez Cortizas, A., Soo Lim, H., & Appleby, P. G. (2013). Chronostratigraphy of the sedimentary record of Limnopolar Lake, Byers Peninsula, Livingston Island, Antarctica. *Antarctic Science, 25,* 198–212.

Turner, J., Colwell, S. R., Marshall, G. J., Lachlan-Cope, T. A., Carleton, A. M., Jones, P. D., Lagun, V., Reid, P. A., & Iagovkina, S. (2005). Antarctic climate change during last 50 years. *International Journal of Climatolology, 25*, 279–294.

Vieira, G., Bockheim, J., Guglielmin, M., Balks, M., Abramov, A. A., Boelhouwers, J., Cannone, N., Ganzert, L., Gilichinsky, D. A., Goryachkin, S., López-Martínez, J., Meiklejohn, I., Raffi, R., Ramos, M., Schaefer, C., Serrano, E., Simas, F., Sletten, R., & Wagner, D. (2010). Thermal state of permafrost and active-layer monitoring in the Antarctic: advances during the International Polar Year 2007-09. *Permafrost and Periglacial Processes, 21 (2),* 182–197.

Vonk, J. E., Tank, S. E., Bowden, W. B., Laurion, I., Vincent, W. F., Alekseychik, P., Amyot, M., Billet, M. F., Canário, J., Cory, R. M., Deshpande, B. N., Helbig, M., Jammet, M., Karlsson, J., Larouche, J., MacMillan, G., Rautio, M., Walter Anthony, K. M., & Wickland, K. P. (2015). Review and Syntheses: Effects of permafrost thaw on Arctic aquatic ecosystems. *Biogeosciences, 12,* 7129–7167.

Watcham, E. P., Bentley, M. J., Hodgson, D. A., Roberts, S. J., Fretwell, P. T., Lloyd, J. M., Larter, R. D., Whitehouse, P. L., Leng, M. J., Monien, P., & Moreton, S. G. (2011). A new relative sea level curve for the South Shetland Islands, Antarctica. *Quaternary Science Reviews, 30,* 3152–3170.

Yoon, H. I., Han, M. W., Park, B. K., Oh, J. K., & Chang, S. K. (1997). Glaciomarine sedimentation and paleo-glacial setting of Maxwell Bay and its tributary embayment, Marian Cove, South Shetland Island, West Antarctica. *Marine Geology, 140,* 265–282.

Table 1. Main limnological and morphological data of the lakes studied in this research.

Lake	Latitude/ Longitude	Altitude (m asl)	Catchment area (km^2)	Core length (cm)	Geomorphological setting
L5	62º 14' 19'' N 58º 45' 27'' W	35	0.28	43	Depression next to a costal cliff connecting with the Holocene marine terraces
L6	62º 14' 22'' N 58º 44' 40'' W	39	0.39	98	Depression next to a costal cliff connecting with the Holocene marine terraces
L11	62º 14' 15'' N 58º 43' 45'' W	67	0.11	24	Lake undergoing a process of terrestritification (peatland) at the foot of a moraine ridge
L12	62º 13' 26'' N 58º 45' 42'' W	102	0.05	37	Lake located in a depression dammed by a moraine at the valley bottom in a still glaciated valley
L13	62º 13' 26'' N 58º 45' 35'' W	103	0.03	30	Lake located in a depression at the valley bottom in a still glaciated valley

Table 2. Results of AMS ^{14}C dating with samples from the three lakes with living and subfossil mosses.

Lake -core	Lab code	Sediment depth (cm)	Material	$\delta^{13}C$ (‰)	Conventional radiocarbon age (yr BP)	Calibrated age (cal yr BP) (2σ)
L5	CNA2435-2-1	5	bulk sediment	-21.6	1490 ± 35	1340 ± 45
	β-335038	42	bulk sediment	-19.7	2830 ± 30	2890 ± 55
L6	β-335036	94	bulk sediment	-25.1	7150 ± 30	7940 ± 45
L11	CNA2438-2-1	18	bulk sediment	-27.4	3495 ± 35	3720 ± 110
L12	β-335037	34	moss	-22.9	2450 ± 30	2440 ± 80
L13	CNA2439-2-1	21	bulk sediment	-20.8	4165 ± 35	4660 ± 90

Table 3. Mean average major element glass compositions (as weight percent oxides, normalised to anhydrous composition) and standard deviations (SD) of sampled tephra layers from lakes L5 and L6.

Lake Core	Tephra Layer	Depth (cm)	Na2O		MgO		SiO2		Al2O3		K2O		TiO2		SO2		CaO		FeO		MnO		P2O5		Total
			wt%	σ	wt%	σ	wt%	σ	wt%	σ	wt%	σ	wt%	σ	wt%	σ	wt%	σ	wt%	σ	wt%	σ	wt%	σ	
L6	C	16	4.28	0.55	3.95	0.62	54.00	1.85	15.70	0.82	0.65	0.17	2.32	0.27	0.09	0.06	7.93	0.97	10.48	0.78	0.19	0.03	0.42	0.07	98.39
L6	B	26	4.26	0.48	4.37	0.80	54.99	1.82	16.08	0.75	0.69	0.18	1.76	0.28	0.03	0.02	8.25	1.36	9.05	0.87	0.19	0.03	0.32	0.10	98.20
L6	A	86	4.29	0.47	4.07	0.39	53.19	1.40	15.70	0.61	0.58	0.12	2.38	0.12	0.07	0.04	8.27	0.67	10.80	0.47	0.21	0.02	0.42	0.05	98.23
L5	C	4	4.14	0.55	4.14	0.56	54.74	1.09	14.80	0.85	0.75	0.11	2.28	0.32	0.02	0.01	7.91	0.70	10.64	0.90	0.20	0.02	0.38	0.06	97.62
L5	B	15	4.11	0.64	4.54	1.07	53.71	1.90	14.70	1.12	0.70	0.16	2.38	0.47	0.03	0.02	8.37	1.02	10.86	1.27	0.21	0.04	0.39	0.10	97.92
L5	A	17	4.43	0.47	4.24	0.17	53.04	0.41	14.67	0.67	0.64	0.05	2.74	0.24	0.03	0.01	8.00	0.20	11.49	0.63	0.22	0.03	0.51	0.13	98.38

Figure captions

Figure 1. Location of Barton Peninsula within the South Shetland Islands and the Antarctic Peninsula region (left), with the distribution of the studied lakes in Barton Peninsula (right).

Figure 2. Pictures of the lakes cored in Barton Peninsula.

Figure 3. Geomorphological sketch with the distribution of the main landforms and deposits in Barton Peninsula (modified from Serrano & López-Martínez, 2004).

Figure 4. Pictures of the cores with the available ^{14}C dates for the sedimentary sequences and the analyzed tephra layers in L5 and L6 cores (numbers denote the sediment units).

Figure 5. Matrix glass compositions of sampled visible tephra layers from (a,c) lake L6 and (b,d) lake L5, expressed as anhydrous oxides. Black crosses (lower left) represent uncertainties (2σ) based on standard repeats. For comparison, shaded regions correspond to the range of published tephra compositions for T3 (grey) and T1/T2 (light/dark orange) layers from Byers Peninsula (Liu et al. 2016).

Figure 6. Principal Component Analysis (PCA) visualisation of the first two principal components (PC; 93% of the variance) of standardised matrix glass compositions from Barton L5 and L6 tephras (this study) and Byers Peninsula T1-3 tephras (Liu et al., 2016). PCA scores of each oxide (magnitude and direction) are shown in the upper right. Bold large circles show the centroid for each sample.

Figure 7. Geomorphological sketch of Barton Peninsula and distribution of the basal ^{14}C dates presented in this paper as well as the cosmogenic ^{36}Cl exposure dates (in red) reported by Seong et al (2009).

Figure 8. Glacial evolution in Barton Peninsula after the deglaciation of Maxwell Bay with the development of the: (A) Outer moraine complex, (B) Intermediate moraine complex, (C) Inner moraine complex, (D) Present-day glacier extent.

Figure 9. Volcanic source of the Barton tephra deposits. Comparison of glass compositions of sampled tephras (symbols) to bulk rock compositional fields of nearby volcanic centres (redrawn from Fretzdorff & Smellie, 2002; Liu et al., 2016), including Penguin Island (white), King George Island (pale grey), Deception Island (grey; glass compositions in dark grey), and Sail Rock (black).

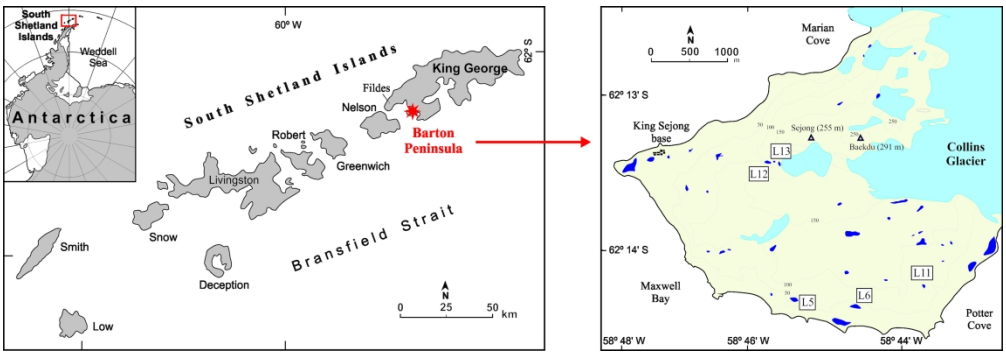

Figure 1. Location of Barton Peninsula within the South Shetland Islands and the Antarctic Peninsula region (left), with the distribution of the studied lakes in Barton Peninsula (right).

252x87mm (300 x 300 DPI)

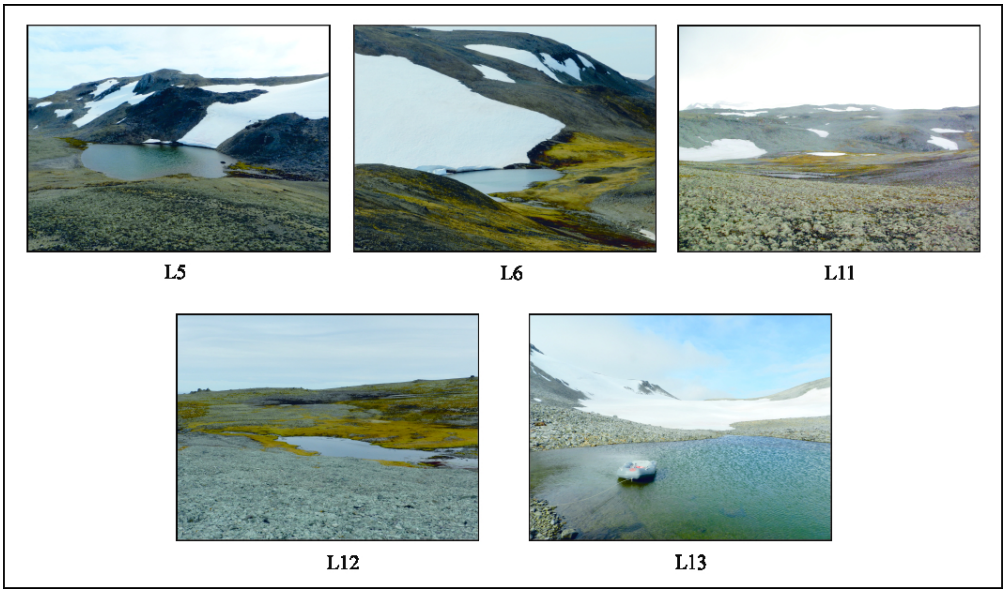

Figure 2. Pictures of the lakes cored in Barton Peninsula.

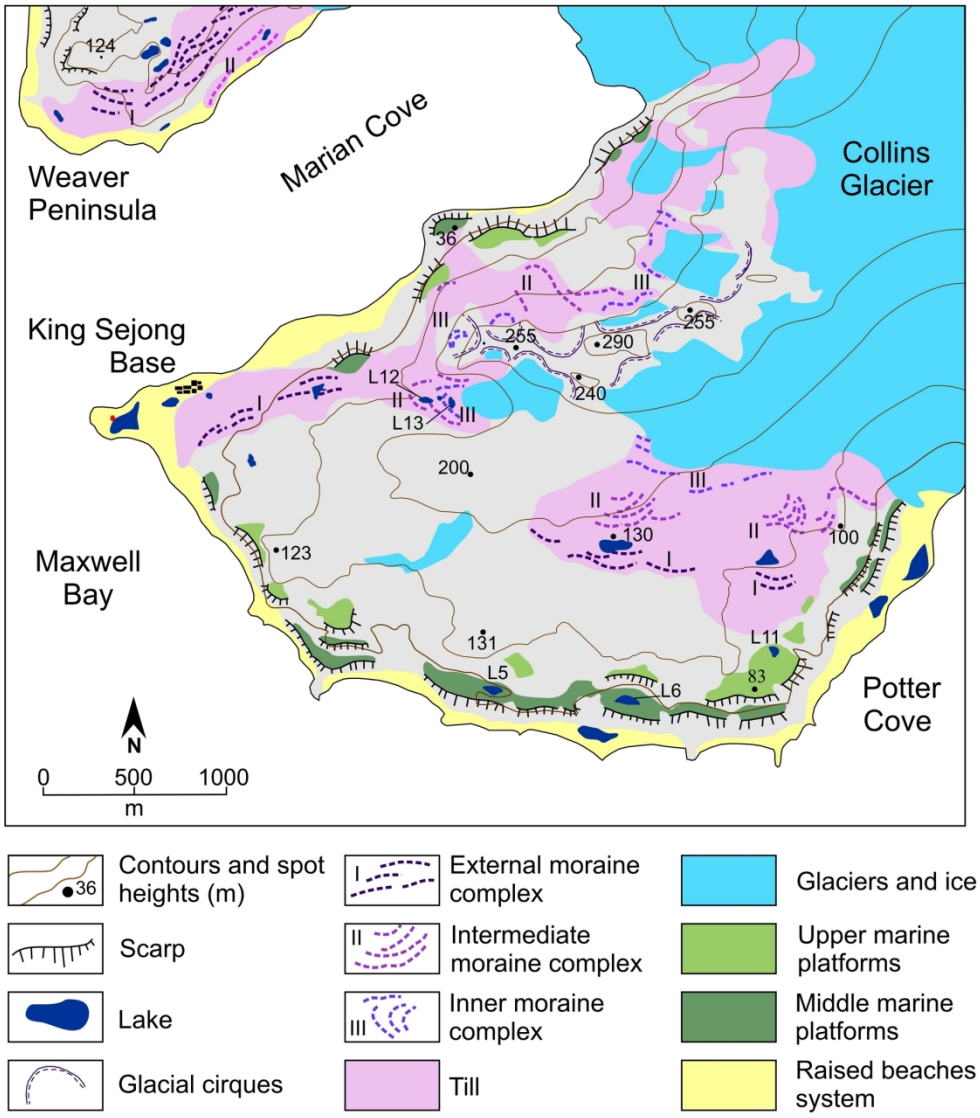

Figure 3. Geomorphological sketch with the distribution of the main landforms and deposits in Barton Peninsula (modified from Serrano & López-Martínez, 2004).

167x192mm (300 x 300 DPI)

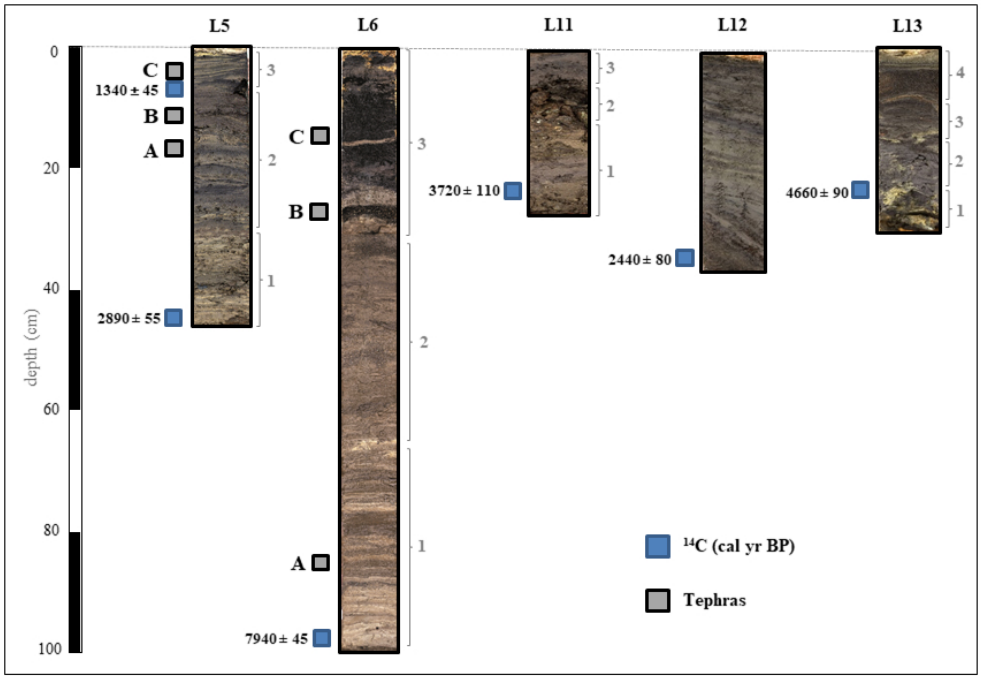

Figure 4. Pictures of the cores with the available 14C dates for the sedimentary sequences and the analyzed tephra layers in L5 and L6 cores (numbers denote the sediment units).

229x170mm (96 x 96 DPI)

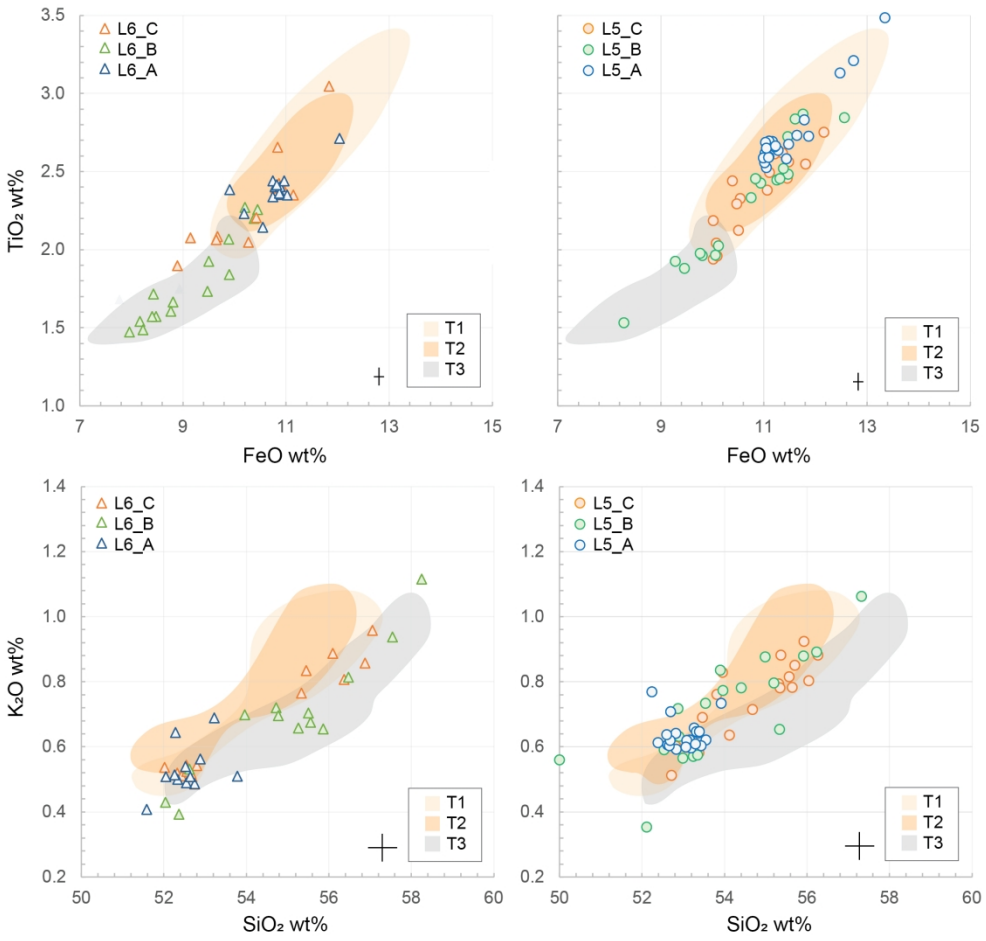

Figure 5. Matrix glass compositions of sampled visible tephra layers from (a,c) lake L6 and (b,d) lake L5, expressed as anhydrous oxides. Black crosses (lower left) represent uncertainties (2σ) based on standard repeats. For comparison, shaded regions correspond to the range of published tephra compositions for T3 (grey) and T1/T2 (light/dark orange) layers from Byers Peninsula (Liu et al. 2016).

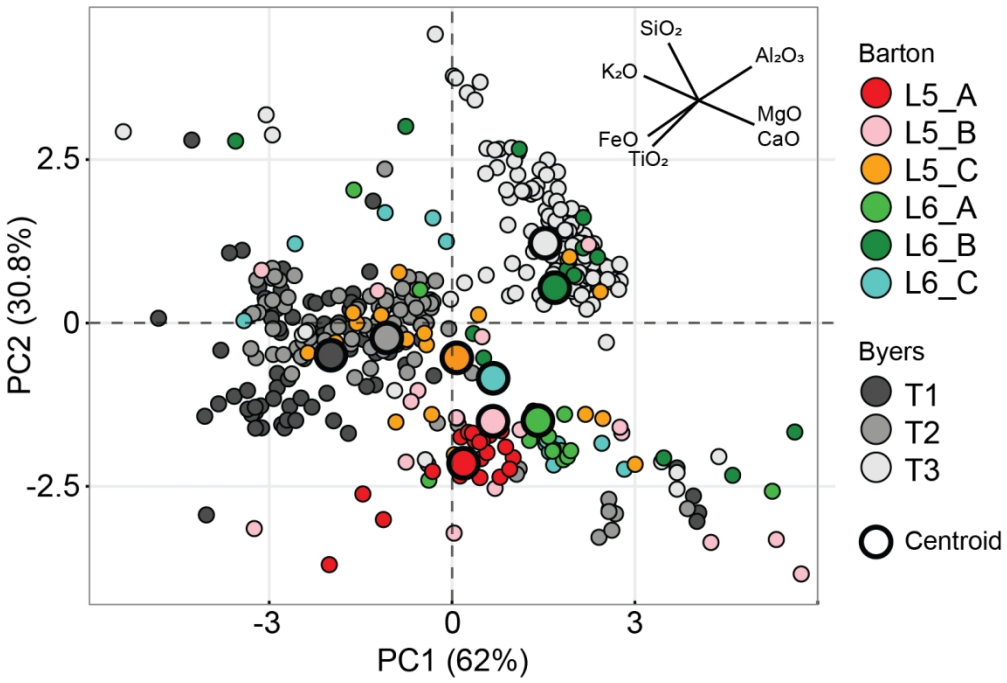

Figure 6. Principal Component Analysis (PCA) visualisation of the first two principal components (PC; 93% of the variance) of standardised matrix glass compositions from Barton L5 and L6 tephras (this study) and Byers Peninsula T1-3 tephras (Liu et al., 2016). PCA scores of each oxide (magnitude and direction) are shown in the upper right. Bold large circles show the centroid for each sample.

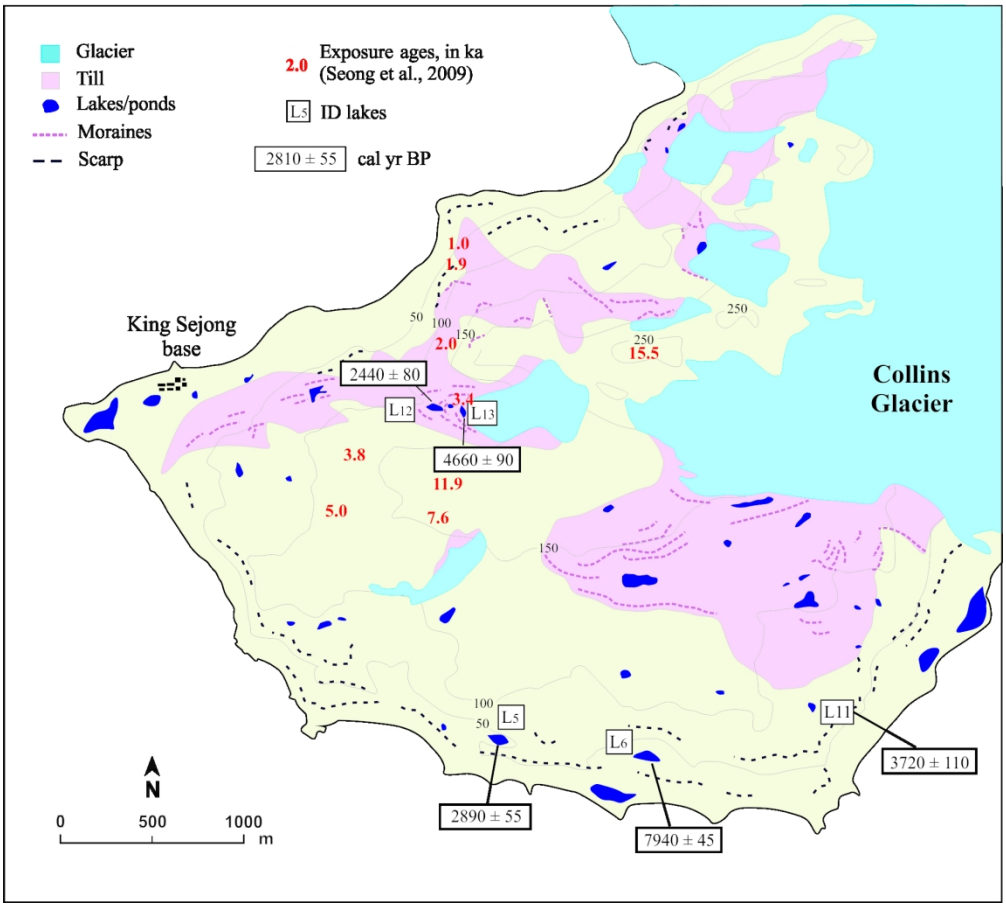

Figure 7. Geomorphological sketch of Barton Peninsula and distribution of the basal 14C dates presented in this paper as well as the cosmogenic 36Cl exposure dates (in red) reported by Seong et al (2009).

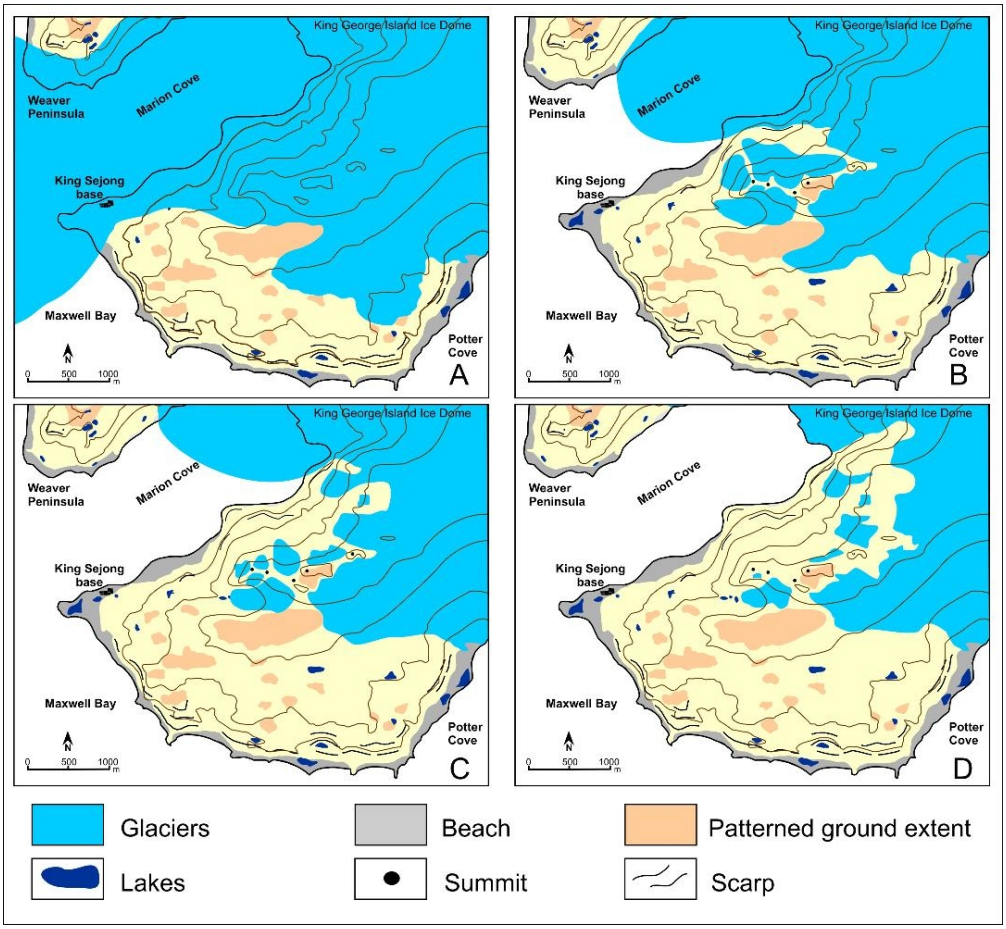

Figure 8. Glacial evolution in Barton Peninsula after the deglaciation of Maxwell Bay with the development of the: (A) Outer moraine complex, (B) Intermediate moraine complex, (C) Inner moraine complex, (D) Present-day glacier extent.

381x351mm (72 x 72 DPI)